Research Article | Vol. 28, No. 13 / 22 June 2020 / Optics Express 19413
Optics EXPRESS

Fabrication of moiré on curved surfaces

ARTIN SABERPOUR,[1,*] ROGER D. HERSCH,[2] JIAJING FANG,[1] RHALEB ZAYER,[1] HANS-PETER SEIDEL,[1] AND VAHID BABAEI[1]

[1]Computer Graphics Department, Max Planck Institute for Informatics, 66123 Saarbrücken, Germany
[2]School of Computer and Communication Sciences, École Polytechnique Fédérale de Lausanne (EPFL), CH-1015 Lausanne, Switzerland
[*]asaberpo@mpi-inf.mpg.de

Abstract: Moiré is an appealing visual effect observable when two or more repetitive patterns are superposed. Fabrication of moiré effects has already proven to be useful in a range of applications, from art to engineering. Here, we introduce a method for designing and fabricating level-line moirés on curved surfaces. These moiré shapes are obtained by superposing a partly absorbing layer and a layer formed by an array of cylindrical lenses or by two layers of cylindrical lenses. We formulate the problem of placing an array of cylindrical lenses on a curved surface as a design problem with a small number of dimensions. The range of possible solutions can therefore be explored by a human observer. We demonstrate the quality of our method by rendered simulations and by fabrication. The resulting static displays can be manufactured using different fabrication techniques, from multi-material 3D printing to molding.

1. Introduction

Moiré is an intriguing phenomenon observable when spatial patterns are superposed [1]. It has broad implications in a range of scientific disciplines, from optical interferometry [2] to atomic lattice interaction [3]. Moreover, moiré theory [1] can be used to design and fabricate fascinating visual effects. Physical realization of moiré patterns has many applications from art and decoration to anti-counterfeiting.

Synthesis and fabrication of moiré shapes such as faces, text, graphic symbols or ornaments has until now only be carried out on planar 2D surfaces. Thanks to recent advances in 3D fabrication techniques, we foresee a great potential in extending moiré effects to a wide range of real-life non-planar objects. The proposed surface moiré technology can be applied as a means of preventing counterfeits. For example it is possible to print the logo of a company as moiré on an object that is printed in 3D. In another case, our proposed moiré synthesizing method could be used to produce a tag validating that an object is 3D printed with a specific type of printer. Such a moiré tag would make it harder to counterfeit the object with other 3D printers.

In the present contribution, we introduce *curved surface moiré* and explore different aspects of its design and fabrication. We show that a straightforward extension to surfaces, inspired by the method of content-adaptive lenticular prints [4], does not yield satisfactory results. Our proposed solution expresses the layout of the lenses on the curved surface as a two-dimensional design space that can be explored subjectively by a human observer. We simulate compelling moiré effects and fabricate them primarily using multi-material 3D printing. For a special single-material type of moiré, coined *dual-lens moiré* [5,6], we use additional fabrication techniques, such as molding, hinting at the potential of our method for mass manufacturing.

1.1. Related work

We briefly review several approaches that are closely related to our work.

#393843 https://doi.org/10.1364/OE.393843
Journal © 2020 Received 17 Apr 2020; revised 27 May 2020; accepted 27 May 2020; published 16 Jun 2020

Optics EXPRESS

1.1.1. Moiré synthesis

Printing is the most common way of creating a wide range of moiré effects. Usually, a *revealer* layer (often a grating of horizontal transparent lines) is printed and superposed on a *base* layer incorporating repetitive structures. The superposition results in a message, motif or image that can be animated by having the revealer sampling successive positions of the base.

Orientations, periods as well as the moiré intensity profile of moiré fringes can be modeled by considering the superposition of the layers as a multiplication in the spatial domain, and therefore as a convolution in the spatial-frequency domain [7], [[1], Chapters 2, 4]. The so-called 1D moiré is obtained by smoothly shifting the revealer on top of a base made of repetitive bands containing each the vertically compressed motif that is to appear as moiré shape. The change of relative phase between revealer and base yields animated moiré symbols and motifs having different speeds and orientations [8]. The use of a 2D lens array acting as a revealer sampling a 2D array of microimages in order to obtain a 2D moiré has been known for a long time [9,10]. When the revealer samples successive portions of the base, 1D or 2D moiré shapes move dynamically along known trajectories.

Recently, micro-fabrication techniques have been used to realize moiré patterns at where the revealing layer [11,12] or both the revealing and base layers [5,6] are made of microlens arrays. Our work can be thought of as the extension of lens-based, level-line moiré to curved surfaces.

1.1.2. Synthesis of caustics

Caustics are obtained by devices that reflect or refract light into a surface according to a desired intensity profile, for example a multi-intensity image. Researchers fabricated slabs that guide the incoming light to form a desired distribution on a receiving surface through optimizing the slopes of a set of microfacets [13]. This work is later extended to refractive surfaces made of a collection of curved patches [14]. Additional optimizations are introduced to stress the importance of surface continuity in order to improve the contrast of the resulting caustics [15–17]. In the present contribution, we show that high-quality curved surface moirés also require the continuity of the underlying geometry. Unlike the static intensity images generated by caustics, the surface moiré exhibits a dynamic nature and can be embedded in a wide range of curved surfaces.

1.1.3. Light field display fabrication

The moiré view-dependent characteristics can be best described using light fields. Our fabricated device belongs to the *automultiscopic* display category [18] making it, to the best of our knowledge, the first free-form automultiscopic display. Automultiscopic displays provide 3D vision cues, such as disparity and motion parallax, without cumbersome, special glasses. A predominant automultiscopic technology is based on parallax barriers that split the rays emitted towards the eyes. Our work is closely related to light-field displays embodied by lenticular prints [4]. Compared to the opaque barriers, lenticular lenses offer a high light throughput efficiency. We draw insights from this work but show that its extension to curved surfaces does not yield high quality moirés.

1.2. Paper overview

Of particular interest in the context of this manuscript, is a special class of moiré, namely, the level-line moiré, see [19] and [[1], Chapter 11]. Readers unfamiliar with the level-line moiré are referred to Appendix A. In Sections 2 and 3, we explain the principles of lens-based level-line moiré design, accounting for free parameters such as lens radius or focal length. In Section 4 we introduce our method of positioning the base and revealing layer surfaces relative to each other. In Section 5, we show that our framework is extendable to a special type of single-material moiré where both base and revealing moiré layers are made of cylindrical lens arrays [6]. In Section 6

Optics EXPRESS

we show a variety of examples, both simulated and fabricated, demonstrating high-quality moiré effects on different curved surfaces.

Given the dynamic nature of the moiré, we highly recommend the reader to watch the *visualizations* (hyperlinks to the videos) for viewing the simulated and fabricated results.

2. Lens-based planar moiré

In level-line moiré, the base layer is calculated from an *elevation profile* extracted from a letter, motif or image (Fig. (1(a))). It is formed by horizontally laid out replicated line patterns, shifted vertically in proportion to the elevation at that location (Fig. 1(b)). Superposing a rectilinear line grating made of transparent lines (Fig. (1(c))) on this base layer produces a moiré whose constant colors or intensities follow the *level set* of the elevation profile, i.e. its level lines (Fig. 1(d)).

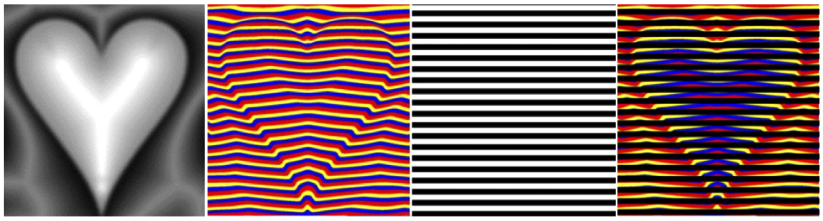

Fig. 1. (a) Elevation profile extracted from a gray-level image, (b) base layer shifted according to the elevation profile, (c) revealing layer, and (d) superposition of the base and revealing layers yielding the level-line moiré (taken with permission from [6]).

In the lens-based planar moiré, the base layer (Fig. 2(b)) is made of unidirectional structures having the same orientation as the revealer's cylindrical lenses, shifted perpendicularly in proportion to an elevation profile. An enlargement of the base-layer band structure is shown in Fig. 2(c). The base must have the same repetition period as the lens pitch, resulting in a one to one correspondence between cylindrical lenses and base layer bands. The superposition of the cylindrical lens array on the base layer yields the moiré. In this moiré, the level lines of the elevation profile are displayed as constant intensity lines (Fig. 2), bottom row). With level-line moirés characterized by the same repetition period of both the base and the revealer, tilting the device has the same effect as shifting the revealer layer over the base layer. The tilting action changes the revealer's phase relative to the base and induces therefore a strong beating effect. This effect can also be compactly represented using sampling moiré method [20]. While there is no quantitative method for moiré quality, a superior moiré is readily distinguishable by an observer through its high-contrast smoothly evolving beating effects when viewed from different directions. On the other hand, a poor-quality moiré exhibits low-contrast, irregular waves upon tilting. To show this visual criterion, Fig. 3 illustrates a comparison between a high and low quality level-line moiré.

A lens array (Fig. 4(a)) reveals the moiré with a much higher light efficiency than a black and clear grating. While the grating blocks a portion of the light, the lens array only redirects it. Recently, the use of flat cylindrical lens arrays for creating high-quality 1D moirés [5,11] and level-line moirés [6] has been demonstrated. Here, we review the relevant equations of a lens system and derive the relationship between lens parameters [6].

In a cylindrical lens (Fig. (4(b))), there is a relationship between the lens radius r, the lens pitch (or width) w and its sag-height h:

$$(r - h)^2 = r^2 - (w/2)^2 \tag{1}$$

Optics EXPRESS

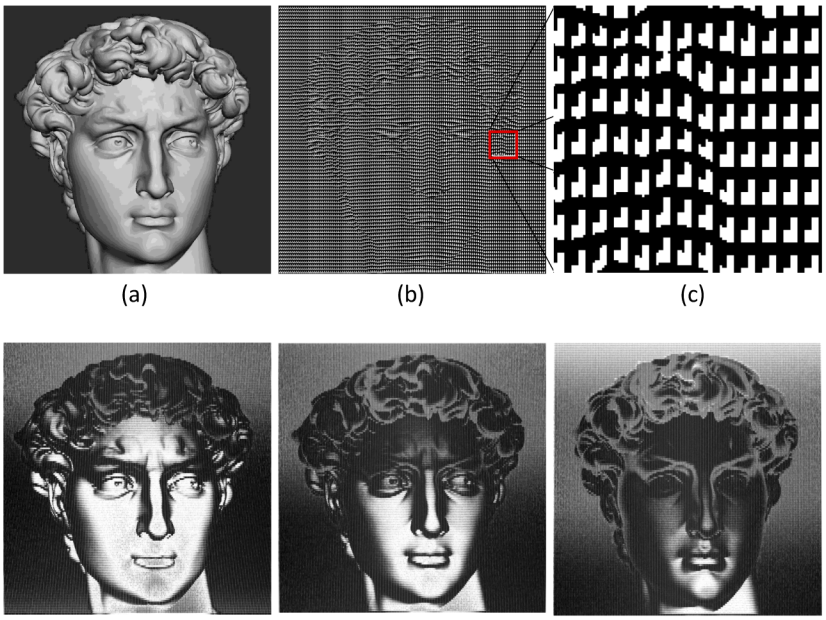

Fig. 2. Top row: (a) elevation profile formed by a gray-level image, (b) base layer shifted according to the elevation profile, (c) a closer view of the base layer. Bottom row: superposition of the base and revealing layers yielding the level-line moiré, shown at different tilt angles.

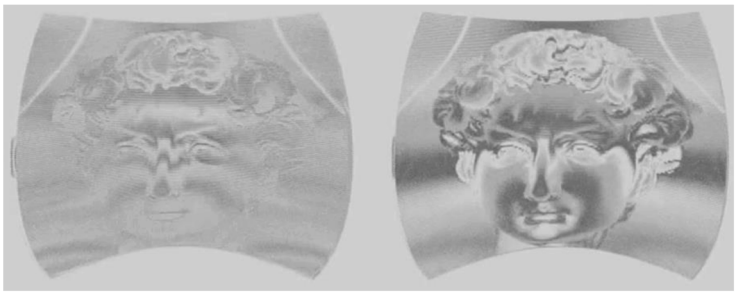

Fig. 3. Comparison between a low (left) and high (right) quality level-line moiré, see Visualization 1

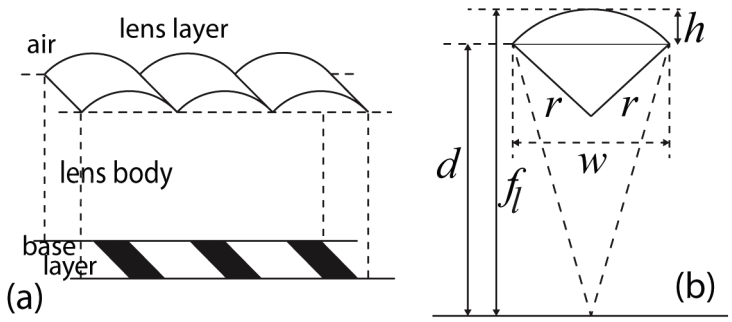

Fig. 4. (a) A cylindrical lens array on top of a base layer. (b) Cross section of a single cylindrical lenslet with r: lens radius, w: lens pitch (or width), h: sag-height, f_l: focal length, and d: lens body thickness.

Optics EXPRESS

The focal length f_l is given by [21]:

$$f_l = \frac{\eta_l}{\eta_l - \eta_{air}} r \tag{2}$$

where η_l and η_{air} are the indices of refraction of the lens material and of the air, respectively. For many polymers, including our materials, we can assume a refractive index of 1.5, thus $f_l = 3r$. For the synthesis of a revealer, once the lens pitch w has been set according to the base layer repetition period, the only additional parameter that can be freely chosen within certain bounds is the lens curvature radius r. The curvature radius defines the angular field of view, see Section 3.2.

The sag-height h enables obtaining the center of the lens surface, useful for creating the mesh that is used for fabrication. The sag-height is obtained from Eq. (1):

$$h = r - \sqrt{r^2 - (\frac{w}{2})^2} \tag{3}$$

In contrast to moirés on curved surfaces, only a single cylindrical lens pitch is present on level-line moirés laid out on a planar surface.

3. 3D extension of lens-based moiré

The input to our method is a 2D planar base layer derived from an elevation profile of a source image, and a curved surface. In the present work, we limit the discussion to parametric surfaces. In the 3D settings, we call the virtual surface that goes through the intersection points of lens arcs (blue dots in Fig. 5(a)) the *lens-pitch surface* or simply the *pitch surface*. We call the surface of the cylindrical lens array, i.e. the top interface of the moiré device with air, the *lens-arc surface* or simply the *lens surface*. Finally, the *base-layer surface* or *base surface* is the moiré base-layer in 3D. Our proposed surface moiré design takes three steps:

(1) Constructing the *lens-pitch surface* by mapping the planar lens-pitch w_s to the desired surface (step 1 in Fig. 5(a)).

(2) Constructing the *lens-arc surface* by fitting circular arcs to neighboring lens-pitch samples (step 2 in Fig. 5(a)).

(3) Constructing the *base-layer surface* from the lens-pitch surface (step 3 in Fig. 5(a)).

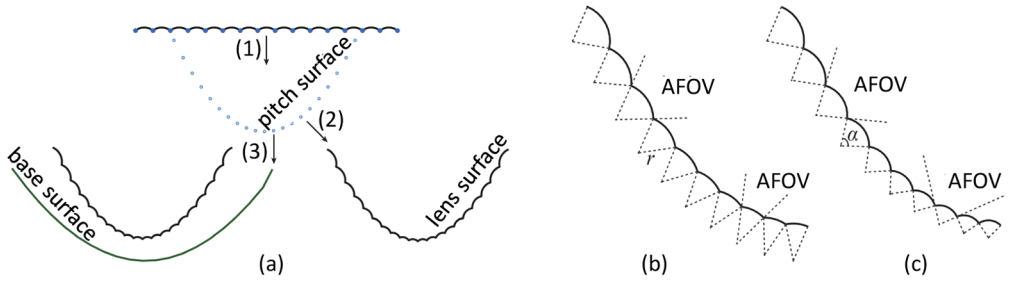

Fig. 5. (a) Three steps in creating surface moiré. (b) Lenses with equal radii (r) are fitted, resulting in different angular field of views (AFOV). (c) By adapting the radius of each lens, the angular field of view α remains constant.

In the following, we explain each step in more details.

Optics EXPRESS

3.1. Lens-pitch surface

In the first step of creating the surface moiré, assuming the input surface is parametric, the lens-pitch surface $\mathcal{P}$ is described by

$$\mathcal{P} : f(u, v). \tag{4}$$

where $f(u, v)$ is a vector function mapping 2D planar positions (u, v) onto (x, y, z) locations in 3D space.

When mapping the equidistant samples of the planar lens-pitch from the parameter domain (u, v) into the lens-pitch surface, distortions are introduced to the formerly equal pitches, resulting in lenses with different focal properties. It is well known from differential geometry [22] that an isometric parameterization exists only for developable surfaces. Therefore, this distortion is in general unavoidable.

3.2. Lens-arc surface

Having computed the spatially-varying lens width, determined by the points of the lens-pitch surface, the next step is to fit the lens-arc surface to this underlying grid. For each individual lens pitch w from the previous step, there is still one degree of freedom: the lens radius r. At the first glance, one can use this degree of freedom to fit equi-radius arcs to the spatially-varying widths (Fig. 5(b)). This has the desirable effect of making the focal length of all lenses equal. The downside, however, is that this leads to lenses with a wide range of angular fields of view that degrade the quality of the resulting moiré.

We use instead this degree of freedom to fit arcs with radii that generate lenses with equal angular field of views (AFOV or α) (Fig. 5(c)). For a fixed angular field of view α, Eq. (5) shows that the lens radius r is proportional to the lens width w. The focal length f_l is therefore also proportional to the lens width w. According to Fig. 4(b),

$$sin(\alpha/2) = \frac{w}{2r}. \tag{5}$$

3.3. Base-layer surface

Having synthesized the lens-arc surface, the final and most important step for creating the surface moiré is to create the base-layer surface. The main challenge is that the inevitable distortions in the lens-pitch surface have an effect on the lens-surface, resulting in spatially-varying lens radii. A careful look at designing flat lenticular (cylindrical) prints [4] reveals a similar challenge: how to adjust the lenses to the spatial frequency of their base? They adapt the focal length of each

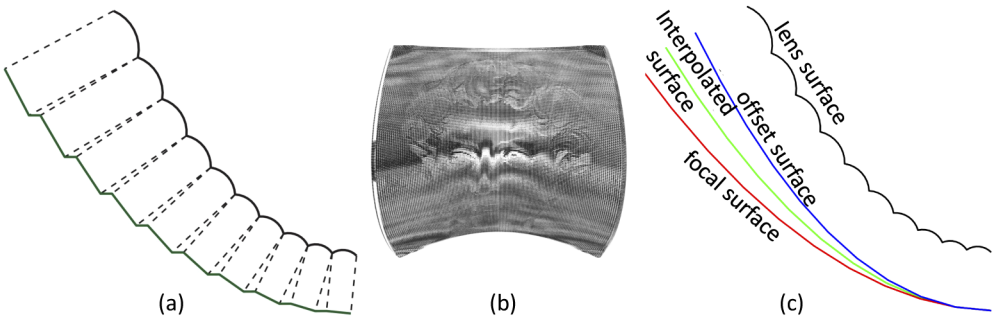

Fig. 6. (a) Inspired by [4], we design a base surface (in green) that is both parallel to the individual lenses and in their focal plane. (b) The rendered simulation of such a design. The nonsmooth base-layer causes artifacts. (c) For a given lens surface, we can compute the offset surface (blue), the focal surface (red) and one of the interpolation surfaces (green).

Optics EXPRESS

lens to its radius while keeping the base-layer facets perfectly parallel to the planar lens-pitch layer facets. Although the curved lens-pitch surface of curved surface moirés differs from the flat lens-pitch surface of planar lenticular prints, the problem is similar.

We therefore compute the base-layer surface from the lens surface in the same manner as in the case of adaptive lenticular prints [4], by placing the surface patches parallel to the corresponding lens-pitch elements at a distance corresponding to their focal length. A typical cross section of the the resulting construction is shown in Fig. 6(a), in this case for a saddle surface. The rendered simulation of the resulting lens-based moiré is shown in Fig. 6(b) (details of our renderings are discussed in Section 6).

Despite each individual lens focusing on a parallel surface segment, the discretization in the base layer introduces aliasing-like artifacts in the form of undesired moiré noise. In the next section, we put forward our solution for designing optimal, smooth base-layer surfaces.

4. Base-layer surface design

The observations in Section 3.3 leads to our main insight in designing surface moiré: the optimal base-layer surface must be parallel to the lens surface *and* stay in focus *while* avoiding discrete jumps. However, *parallelity* and variable *focality*, for most continuous surfaces, are conflicting objectives (Fig. 6(c)). A notable exception is the plane where the base layer is both parallel and perfectly in focus, explaining the high quality of the planar moiré. Thus, for a given lens surface, we propose to compute its corresponding *focal surface*, i.e. the surface that is smoothly in focus as well as its *offset surface(s)*, i.e. surfaces whose elements are strictly parallel to the corresponding lens-pitch surface elements. We conjecture that the optimal base-layer surface lies *in between* these two surfaces. Therefore, we introduce a formulation that embeds the optimal base surface in a low dimensional *design space* thereby enabling its rapid exploration.

4.1. Offset surface

Given our lens-pitch surface $\mathcal{P}$ (Eq. (4)), the offset surface $\mathcal{Q}$ of $\mathcal{P}$ is defined as a surface whose points are at a distance d from their corresponding points on $\mathcal{P}$

$$\mathcal{Q} : g(u, v; d) = f(u, v) - d\, n_f(u, v) \tag{6}$$

where the parameter d implies that $\mathcal{Q}$ is not unique, and $n_f(u, v)$ is the unit surface normal vector of $\mathcal{P}$ defined as

$$n_f = \frac{f_u \times f_v}{\|f_u \times f_v\|} \,. \tag{7}$$

with $f_u = \partial f / \partial u$ and $f_v = \partial f / \partial v$ being the partial derivatives of f.

4.2. Focal surface

For a given lens surface, its corresponding *focal surface* is a smooth surface continuously in focus. We compute the focal surface as a *continuous* function of the lens-pitch surface assuming that any point on the lens-pitch surface is the midpoint of the two end points of a lens. If all such lenses on the lens surface had the same default radius r_s (and default pitch w_s), the focal surface would be equal to one of the offset surfaces with a distance d equal to the unique focal length of all lenses. Due to the distortion, the radius changes along the surface depending on the surface curvature. Once that the AFOV has been fixed in the lens-arc surface construction stage, both the standard pitch w_s and its corresponding radius r_s are distorted with the same factor. According to the properties of the cylindrical lenses (Fig. 4(b) and Eq. (2)), and the fact that $w/w_s = r/r_s$, the focal surface $\mathcal{R}$ is formulated as:

$$\mathcal{R} : h(u, v) = f(u, v) - n_f(u, v) \frac{\eta_l}{\eta_l - \eta_{air}} \, r_s \, |f_u| \,. \tag{8}$$

Optics EXPRESS

This formulation states that the radius of every lens on the lens surface is distorted from the planar surface radius r_s by the factor $w/w_s = |f_u|$. We explain how this ratio is calculated in Appendix B.

4.3. Interpolated base surface

We explore the space between the offset surfaces $\mathcal{Q}$ and the focal surface $\mathcal{R}$ using a bi-linear interpolation in order to find the base surface $\mathcal{S}$ with the most visible moiré effect. Given that the focal surface is uniquely defined, the design space is made of two free parameters, the relative weight (a) between offset and focal surface and the offset (d). We have therefore

$$\mathcal{S} : s(u, v; a, d) = (1 - a)\ g(u, v; d) + a\ h(u, v)\ . \tag{9}$$

The most important implication of Eq. (9) is that the base layer's design space has only two dimensions. This is very convenient as, in the absence of a reference, the user can simply walk this space and find the two parameters that create the most satisfying moiré effect. According to Fig. 7, the moiré with the base surface identical with the offset surface (i.e. $a = 0$) is superior to the other moirés, for offsets $d = 2r_s$ and $d = r_s$. This seems mainly due to the fact that on a curved surface, the largest part of the moiré is viewed obliquely in respect to the surface normal.

5. Dual-lens surface moiré

An interesting variant of the level-line moiré consists in using an array of cylindrical lenses also for the base layer [6]. The resulting setup combining the two layers of cylindrical lenses has a number of advantages. There is only little light attenuation by the base. The moiré that can be seen in transmission mode shows level lines having the colors of the incident light rays, for example blue light from the sky or green light from the trees. In addition, the device can be 3D printed with a single material and manufacturing methods such as casting can be used.

Let us consider a base formed by horizontal cylindrical lenses. The trajectory of the center line of the lens surface is shifted vertically according to the elevation profile. The shift of the base cylindrical lens grating in respect to the revealer cylindrical lens grating has the effect of selecting incoming light having a different orientation (Fig. 8). The change of orientation of the incoming light rays that pass through the device and reach the eye of the observer creates the level line moiré effect. Simulations of the dual lens surface moiré are shown in Fig. 9 and the fabricated dual-lens moirés are shown in Fig. 10.

Optics EXPRESS

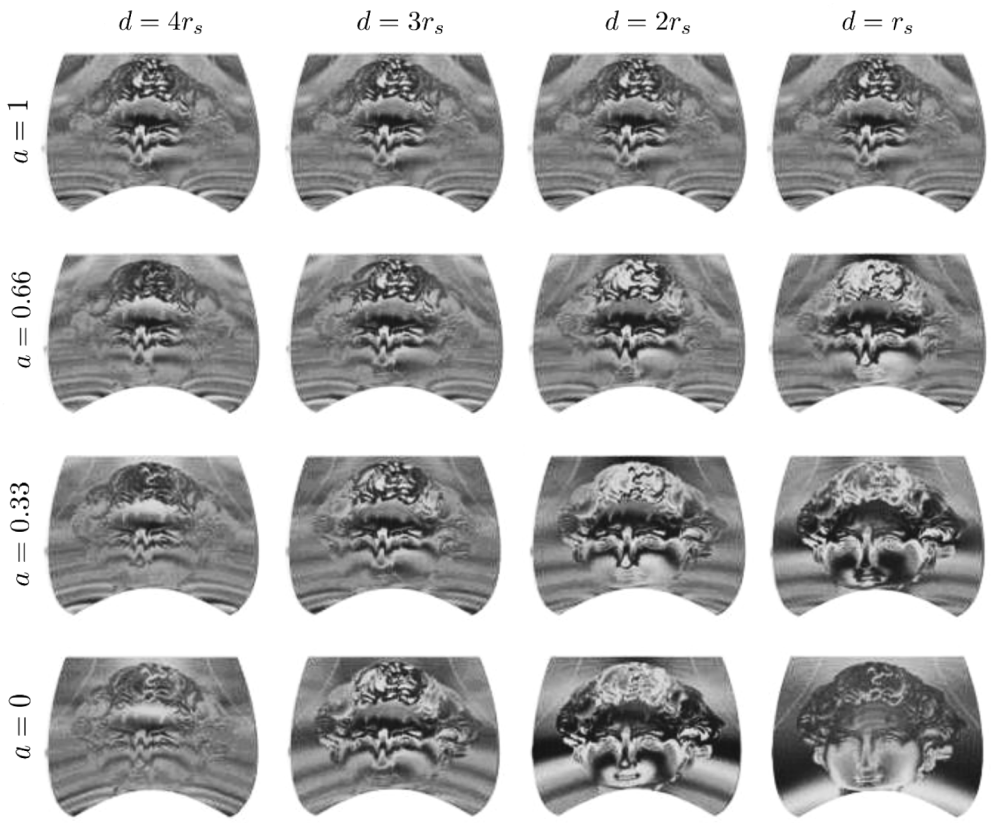

Fig. 7. Design space explored by varying the weighting parameter a and the distance parameter d, see formula 9.

6. Simulation and fabrication

In this section, we show a variety of surface moirés both simulated and fabricated with different elevation profiles and different geometries. As we restrict ourselves to print with only two materials at the same time, as in [4], we choose to use a transparent (clear) material for lenses and a black material for the absorbing parts of the base layer halftone. Therefore, all our results are transmission-based devices and should be illuminated from behind. In all our exploration of different geometries, we found a values near 0 to give the best results (see Fig. 7). This highlights the fact that parallel arrangement of lens and base surfaces is of utmost importance, as also hinted by [6].

Fig. 11 shows a set of different elevation profiles used in rendering and fabrication of our results.

6.1. Simulations

We use Cycles, a physically-based rendering engine based on unidirectional path tracing [23], for all our simulations (128 samples, default settings). As we are rather interested in simulating the dynamism of moiré, and not necessarily the exact appearance, we don't measure the appearance of the employed materials. Accurate appearance prediction of 3D prints is an active research area [24] outside the scope of the current work.

Optics EXPRESS

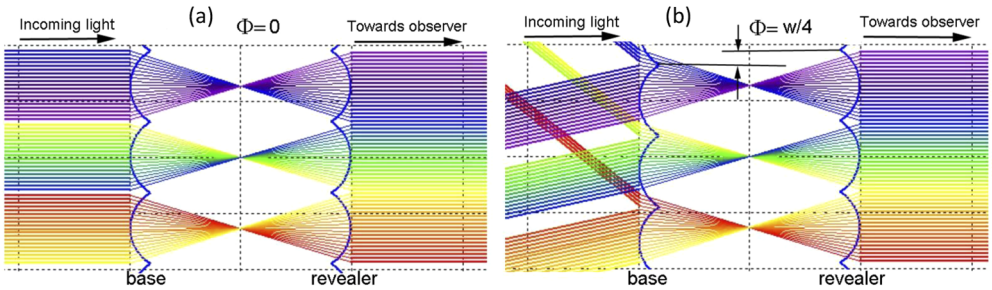

Fig. 8. Cross-section of a transparent device formed by two gratings of transparent cylindrical lenses with light rays oriented towards the eye of an observer having (a) an unshifted base and (b) a base shifted by quarter of the lens repetition period (schematic view).

Fig. 9. Dual-lens surface moiré simulation: (a) and (b) show the Graces level-line moiré on a saddle surface, Visualization 2; (c) and (d) show the David's level-line moiré on a saddle surface,Visualization 3.

We use two default materials, close to our black and clear materials, namely the "Diffuse BSDF" with roughness 1 and refractive index 1.5 for the black material, and "Glass BSDF" with roughness 0 and refractive index 1.5 for the clear material. For the rendering of multi-material moiré the lighting of the scene is ambient light, while for dual-lens surface moiré lateral area lights have been used.

Fig. 9 shows different simulations with various elevation profiles and tilt angles. As it can be seen in these figures, and in the accompanying videos, our designs create dynamically beating moiré shapes as well as highlight and dark areas that move along the surface when viewing the device from different angles.

When tilting the device, the moirés change their shape due to the fact that the angles of the rays from the eye to the cylindrical lenses change in respect to the lens normal. This modifies the sampling locations within the base layer and as a consequence either shrinks or enlarges parts of the moiré shapes.

We don't notice additional undesirable moirés, indicating the usefulness of our framework that comprises constant field of view lens-arc surfaces and the selection of the optimal base surface by design space exploration.

6.2. Fabrication

The new additive fabrication technology is enabling a lot of applications. The level-line moiré created on a curved surface can be attached or pasted onto an object having a curved surface. This is useful both for decoration and for the prevention of counterfeits. In addition to creating moirés on various kinds to geometries, its multi-material capabilities create unprecedented opportunities for designing new systems, e.g. displays [4]. Multi-material 3D printing is our primary fabrication platform for moiré surfaces. While the current additive technology is still

Optics EXPRESS

Fig. 10. (a) and (b) 3D printed dual-lens surface moiré from 2 different angles each, Visualization 8 and Visualization 9 (c) Silicone cast of a dual-lens moiré, illuminated with a green light, from 2 different angles. Visualization 10.

mostly used for prototyping, we also show that there is a potential for mass manufacturing of moiré using molding techniques.

6.2.1. Multi-material 3D printing

Our multi-material 3D printer is an inkjet-based, phase-shift, photopolymer printer [25]. We print all our samples in the *glossy* mode and align the lens's longer axis with the printing direction for a better lens profile reproduction. Fig. 12, Fig. 10(a) and Fig. 10(b) show the samples fabricated with our printer. The movement and the width of dark/highlight moiré bands are very well predicted in our simulation.

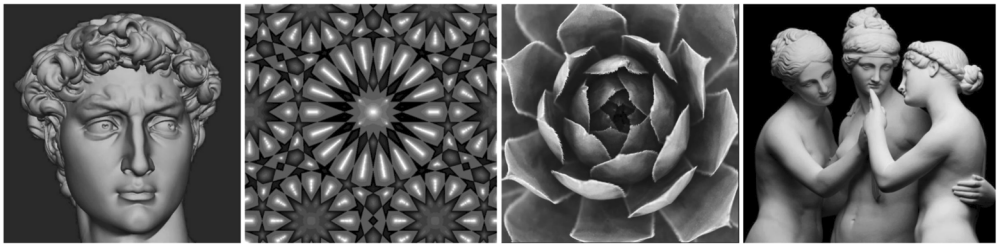

Fig. 11. Elevation profiles. (a) David. (b) Mosque. (c) Flower. (d) Graces.

Optics EXPRESS

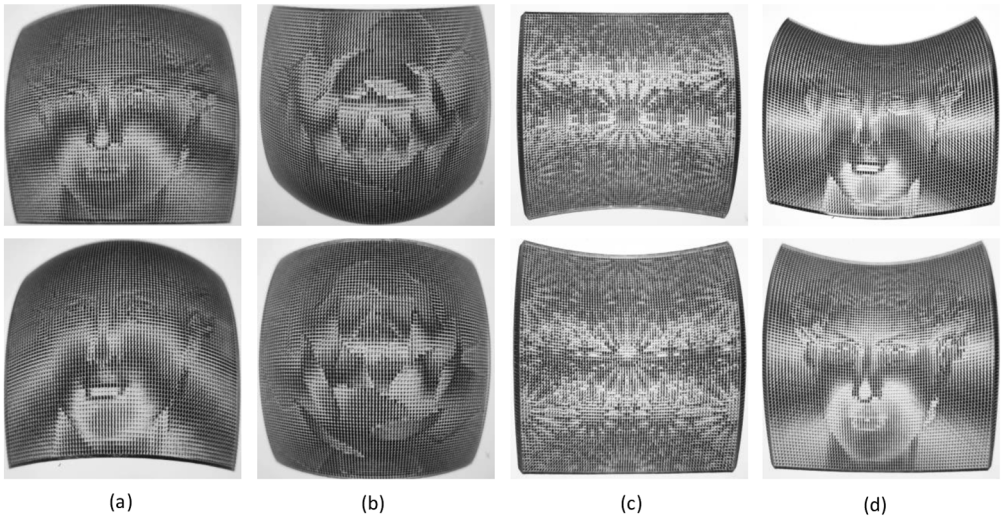

Fig. 12. 3D printed *Parametric surfaces* from 2 different angles each, (a) Paraboloid with David elevation profile, Visualization 4. (b) Paraboloid with Flower elevation profile, Visualization 5. (c) Saddle with Mosque elevation profile, Visualization 6. (d) Saddle with David elevation profile, Visualization 7.

6.2.2. Molding

For designing the mold, we follow the steps proposed by [26] and create the two-piece molds. We use SYLGARD 184 from Dow chemicals, a very clear silicone whose flexibility can be controlled by the ratio of its two components. The high transmittance of the silicone leads to a very clear moiré (Fig. 10(c)), with considerably cleaner beating effects than its 3D printed counterpart (Fig. 10(a) and Fig. 10(b)).

7. Conclusion

We introduced a simple and practical method of extending moiré to curved surfaces. Our results enable creating a novel high-quality effect on surfaces which can be fabricated with different manufacturing approaches. From an artistic point of view, the proposed surface moiré technology exhibits interesting visual properties. It could also be used for the authentication of products and for fighting counterfeits. We plan to streamline our current framework of curved surface moiré rendering in order to explore design variants at interactive rates. Although our low dimensional design space does not require quantifying the moiré quality, more general-purpose light field displays may need to look at this problem. Especially, quantifying the changes in light field quality when going from the original planar display (as a quality landmark) to the surface display could be very useful. Finally, our device is a rigid device which needs to be tilted in order to see the moiré effect. In order to extend the range of effects, we can imagine designing *moiré mechanisms* where, by clasping the device, the revealing surface moves relative to the base surface and changes the appearance of the moiré.

A. Level-line moiré

The theorem of level-line moiré [19], [[1] pp.370-371] states that the level set of an elevation profile appears as moiré lines when superposing an unshifted line grating on a base line grating whose lines are shifted proportionally to the elevation profile. See Fig. 1 for an example of a level-line moiré.

Optics EXPRESS

The general equation of the level-line moiré can be determined by considering the indexed line families of the revealer, the base and the moiré ([27], [[1] sec.11.2 pp.353-360]). As shown in Fig. 13, the transparent lines of the revealer are indexed with $r = 1, 2, 3, \ldots$, the base lines are indexed with $b = 1, 2, 3, \ldots$, and the moiré lines are indexed with $m = \cdots 2, 1, 0, -1, -2 \cdots$. The index m characterizing the moiré fringe lines is equal to the index of the revealer minus that of the base:

$$m = r - b \tag{10}$$

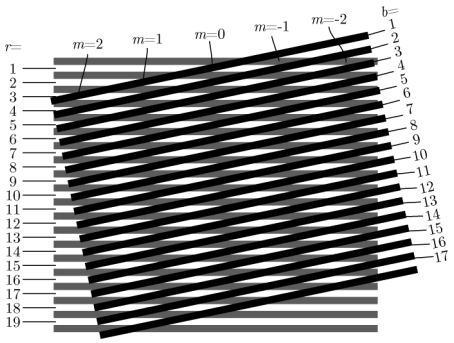

Fig. 13. Superposition of a revealer (gray) and a base (black). The transparent lines of the revealer are indexed with r. The black lines of the base are indexed with b. The moiré fringe lines are indexed with m.

Let us now consider a revealer composed of a periodic grating of lines, which can be straight or curvilinear. Let us define ρ such that the implicit equation of one of these lines is $\rho(x, y) = 0$. The family of revealer lines is thus defined by:

$$\rho(x, y) = r \cdot T_r \tag{11}$$

where r is the index of the lines in the revealer and T_r is the period of the lines in the revealer. For example, $y = r \cdot T_r$ would represent a grating of horizontal lines of period T_r.

Similarly, let us consider a base composed of a periodic grating of lines, which can be straight or curvilinear. Let us define β such that the implicit equation of one of these lines is $\beta(x, y) = 0$. The family of base lines is thus defined by:

$$\beta(x, y) = b \cdot T_b \tag{12}$$

where b is the index of the lines in the base and T_b is the period of the lines in the base.

The implicit equation of the moiré grating can then be obtained by combining Eq. (10), Eq. (11), and Eq. (12):

$$\frac{\rho(x, y)}{T_r} - \frac{\beta(x, y)}{T_b} = m \tag{13}$$

As stated in the level-line moiré theorem suggested in [19] and formulated in [[1], section 11.2, pp. 353-360], the level lines of a surface defined by $z = g(x, y)$ can be obtained by superposing two gratings. As first grating, we consider a revealing grating of horizontal lines and of period T. We consider as the second grating a base layer grating that is a copy of the revealer in which we additionally translate vertically each point (x, y) by a distance equal to $g(x, y)$. The line equations

Optics EXPRESS

of the revealer and the base are respectively:

$$y = r \cdot T \tag{14}$$

$$y - g(x, y) = b \cdot T \tag{15}$$

The resulting moiré is defined by the indicial equation Eq. (10). After replacing r and b thanks to Eq. (14) and Eq. (15), we obtain:

$$m = \frac{y}{T} - \frac{y - g(x, y)}{T} = \frac{g(x, y)}{T} \iff g(x, y) = m \cdot T \tag{16}$$

This means that the moiré lines are indeed level lines of the surface $z = g(x, y)$.

B. Parametric distortion

We are interested in calculating how a 1D segment in the parameter domain (akin to w_s) would deform when mapped to a curve on a surface $f(u, v)$, creating a corresponding segment w. The ratio w/w_s is the same as the ratio of the lens radius r on the curved surface to its radius r_s on the planar surface. Therefore, it gives us the varying radius along the surface and consequently the focal distance for any point on the curved surface f.

In a general setting, let us assume the lens pitch is mapped from a curve $(u(t), v(t))$ in the parametric domain to the parametric curve $\gamma(t) = f(u(t), v(t))$ on the surface $f(u, v)$ (Fig. 14). We first approximate the segment length Δs with chord length $|\Delta\gamma| = |\gamma(t + \Delta t) - \gamma(t)|$ using Taylor expansion:

$$\Delta s \approx |\Delta\gamma| = |\gamma(t + \Delta t) - \gamma(t)| = |\frac{\mathrm{d}\gamma}{\mathrm{d}t}\Delta t + \frac{1}{2}\frac{\mathrm{d}^2\gamma}{\mathrm{d}t^2}(\Delta t)^2| \approx |\frac{\mathrm{d}\gamma}{\mathrm{d}t}|\Delta t. \tag{17}$$

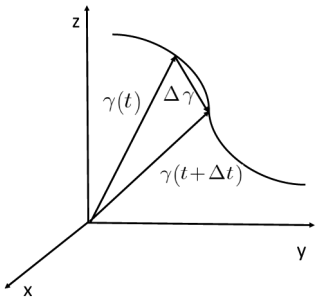

Fig. 14. A parameterized curve $\gamma(t)$ in three dimensional space.

In an infinitesimal setting where $\Delta t \to 0$, the segment length Δs becomes a line element:

$$\mathrm{d}s = |\frac{\mathrm{d}\gamma}{\mathrm{d}t}|\mathrm{d}t = |\dot{\gamma}|\mathrm{d}t = \sqrt{\dot{\gamma}.\dot{\gamma}}\mathrm{d}t. \tag{18}$$

As $\gamma(t) = f(u(t), v(t))$, we have:

$$\begin{aligned} \mathrm{d}s &= |\frac{\mathrm{d}\gamma}{\mathrm{d}t}|\mathrm{d}t \\ &= |f_u\frac{\mathrm{d}u}{\mathrm{d}t} + f_v\frac{\mathrm{d}v}{\mathrm{d}t}|\mathrm{d}t \\ &= \sqrt{(f_u\dot{u} + f_v\dot{v}).(f_u\dot{u} + f_v\dot{v})}\mathrm{d}t \\ &= \sqrt{f_u.f_u.\dot{u}.\dot{u} + 2f_u.f_v.\dot{u}.\dot{v} + f_v.f_v.\dot{v}.\dot{v}}\mathrm{d}t \end{aligned} \tag{19}$$

Recall that we are interested in calculating the ratio $\frac{w}{w_s}$ which corresponds to the line elements $\mathrm{d}s$ and $\mathrm{d}u$, respectively. Parameter v is not concerned as our lenses in the planar case are

Optics EXPRESS

unidirectional, e.g., $v(t) = C$ (C being a constant). Thus, the ratio $|\frac{ds}{du}|$ will give us the distortion at each point on the curve $\gamma(t)$. Hence, given $\dot{v}(t) = 0$, Eq. (19) can be rewritten as:

$$\begin{aligned} ds = \sqrt{f_u.f_u.\dot{u}.\dot{u} + 0 + 0}.dt = |f_u|du \\ \implies |\frac{ds}{du}| = |f_u| \end{aligned} \tag{20}$$

Funding

Max-Planck-Institute for Informatics.

Acknowledgments

We would like to express our gratitude to Willemijn Elkhuizen and Tessa Essers at Delft University of Technology for their kind help with fabrication. We also offer our special thanks to Krzysztof Wolski for his help and comments on improvements of our simulations.

Disclosures

The authors declare that there are no conflicts of interest related to this article.

References

1. I. Amidror, *The Theory of the Moiré Phenomenon: Volume I: Periodic Layers*, vol. 38 (Springer Science & Business Media, 2009).
2. D. Post, B. Han, and P. Ifju, *Moiré Interferometry* (Springer US, 1994), pp. 135–226.
3. C. R. Dean, L. Wang, P. Maher, C. Forsythe, F. Ghahari, Y. Gao, J. Katoch, M. Ishigami, P. Moon, M. Koshino, T. Taniguchi, K. Watanabe, L. Shepard, K J. Hone, and P. Kim, "Hofstadter's butterfly and the fractal quantum hall effect in moiré superlattices," Nature **497**(7451), 598–602 (2013).
4. J. Tompkin, S. Heinzle, J. Kautz, and W. Matusik, "Content-adaptive lenticular prints," ACM Trans. Graph. **32**(4), 1 (2013).
5. T. Walger, T. Besson, V. Flauraud, R. D. Hersch, and J. Brugger, "1d moiré shapes by superposed layers of micro-lenses," Opt. Express **27**(26), 37419–37434 (2019).
6. T. Walger, T. Besson, V. Flauraud, R. D. Hersch, and J. Brugger, "Level-line moirés by superposition of cylindrical microlens gratings," J. Opt. Soc. Am. **37**(2), 209–218 (2020).
7. O. Bryngdahl, "Moiré: formation and interpretation," J. Opt. Soc. Am. **64**(10), 1287–1294 (1974).
8. R. D. Hersch and S. Chosson, "Band moiré images," in *ACM Trans. Graph.*, vol. 23 (ACM, 2004), pp. 239–247.
9. M. Hutley, R. Hunt, R. Stevens, and P. Savander, "The moiré magnifier," Pure Appl. Opt. **3**(2), 133–142 (1994).
10. H. Kamal, R. Voelkel, and J. Alda, "Properties of moiré magnifiers," Opt. Eng. **37**(11), 3007–3014 (1998).
11. V. J. Cadarso, S. Chosson, K. Sidler, R. D. Hersch, and J. Brugger, "High-resolution 1d moirés as counterfeit security features," Light: Sci. Appl. **2**(7), e86 (2013).
12. W. Zheng, S. Shen, Y. Gao, N. Liu, and Y. Liu, "Design methodology for moiré magnifier based on micro-focusing elements," Opt. Express **25**(25), 31746–31757 (2017).
13. T. Weyrich, P. Peers, W. Matusik, and S. Rusinkiewicz, "Fabricating microgeometry for custom surface reflectance," ACM Trans. Graph. **28**(3), 1–6 (2009).
14. M. Papas, W. Jarosz, W. Jakob, S. Rusinkiewicz, W. Matusik, and T. Weyrich, "Goal-based caustics," in *Computer Graphics Forum*, vol. 30 (Wiley Online Library, 2011), pp. 503–511.
15. Y. Yue, K. Iwasaki, B.-Y. Chen, Y. Dobashi, and T. Nishita, "Poisson-based continuous surface generation for goal-based caustics," ACM Trans. Graph. **33**(3), 1–7 (2014).
16. Y. Schwartzburg, R. Testuz, A. Tagliasacchi, and M. Pauly, "High-contrast computational caustic design," ACM Trans. Graph. **33**(4), 1–11 (2014).
17. J. Meyron, Q. Mérigot, and B. Thibert, "Light in power: a general and parameter-free algorithm for caustic design," ACM Trans. Graph. **37**(6), 1–13 (2019).
18. H. Urey, K. V. Chellappan, E. Erden, and P. Surman, "State of the art in stereoscopic and autostereoscopic displays," Proc. IEEE **99**(4), 540–555 (2011).
19. J. S. Marsh, "Contour plots using a moiré technique," Am. J. Phys. **48**(1), 39–40 (1980).
20. S. Ri, M. Fujigaki, and Y. Morimoto, "Sampling moiré method for accurate small deformation distribution measurement," Exp. Mech. **50**(4), 501–508 (2010).
21. E. Hecht, *Optics*, 5e (Pearson Education India, 2017).
22. M. P. do Carmo, *Differential geometry of curves and surfaces*. (Prentice Hall, 1976).
23. Blender, *Blender - a 3D modelling and rendering package*, Blender Foundation, Blender Institute, Amsterdam (2019).

Optics EXPRESS

24. D. Sumin, T. Rittig, V. Babaei, T. Nindel, A. Wilkie, P. Didyk, B. Bickel, J. Křivánek, K. Myszkowski, and T. Weyrich, "Geometry-aware scattering compensation for 3D printing," ACM Trans. Graph. **38**(4), 1–14 (2019).
25. Stratasys, "Objet connex3: How to maximize multi-material and color possibilities," (2014).
26. V. Babaei, J. Ramos, Y. Lu, G. Webster, and W. Matusik, "Fabsquare: Fabricating photopolymer objects by mold 3d printing and uv curing," IEEE Comput. Grap. Appl. **37**(3), 34–42 (2017).
27. G. Oster, M. Wasserman, and C. Zwerling, "Theoretical interpretation of moiré patterns," J. Opt. Soc. Am. **54**(2), 169–175 (1964).